

## Periodic Orbits and Escapes in Dynamical Systems

George Contopoulos · Mirella Harsoula ·  
Georgios Lukes-Gerakopoulos

the date of receipt and acceptance should be inserted later

**Abstract** We study the periodic orbits and the escapes in two different dynamical systems, namely (1) a classical system of two coupled oscillators, and (2) the Manko-Novikov metric (1992) which is a perturbation of the Kerr metric (a general relativistic system). We find their simple periodic orbits, their characteristics and their stability. Then we find their ordered and chaotic domains. As the energy goes beyond the escape energy, most chaotic orbits escape. In the first case we consider escapes to infinity, while in the second case we emphasize escapes to the central “bumpy” black hole. When the energy reaches its escape value a particular family of periodic orbits reaches an infinite period and then the family disappears (the orbit escapes). As this family approaches termination it undergoes an infinity of equal period and double period bifurcations at transitions from stability to instability and vice versa. The bifurcating families continue to exist beyond the escape energy. We study the forms of the phase space for various energies, and the statistics of the chaotic and escaping orbits. The proportion of these orbits increases abruptly as the energy goes beyond the escape energy.

**Keywords** Hamiltonian Systems · Periodic Orbits · Chaotic Motions · Relativity

---

G. Contopoulos  
Research Center for Astronomy and Applied Mathematics, Academy of Athens,  
Soranou Efessiou 4, GR-11527 Athens, Greece  
E-mail: gcontop@academyofathens.gr

M. Harsoula  
Research Center for Astronomy and Applied Mathematics, Academy of Athens,  
Soranou Efessiou 4, GR-11527 Athens, Greece  
E-mail: mharsoul@academyofathens.gr

G. Lukes-Gerakopoulos  
Research Center for Astronomy and Applied Mathematics, Academy of Athens,  
Soranou Efessiou 4, GR-11527 Athens, Greece  
Theoretical Physics Institute, University of Jena, 07743 Jena, Germany  
E-mail: gglukes@gmail.com

## 1 Introduction

The escapes from a dynamical system refer to a problem of basic interest for dynamics: the problem of chaotic scattering. This problem has attracted the attention of many authors in the previous decades (some typical references are by Churchill et al. (1975); Petit and Hénon (1986); Bleher et al. (1988); Eckhardt (1988); Jung and Scholz (1988); Hénon (1989); Contopoulos (1990); Contopoulos and Kaufmann (1992); Ott and Tél (1993); Benet et al. (1996, 1998)).

In particular we found (Contopoulos and Efstathiou 2004) the forms of the escape regions and the escape rates in the simple dynamical system

$$H = \frac{1}{2}(\dot{x}^2 + \dot{y}^2 + x^2 + y^2) - xy^2 = h \quad (1)$$

for various values of the energy  $h$  above the escape energy  $h_{esc} = 0.125$ . We found also regions of orbits that never escape, or escape after a very long time. In particular the stable periodic orbits are surrounded by islands of stability that never escape. This problem is typical of “escapes to infinity”. In fact, similar results were found in general polynomial Hamiltonians representing two perturbed harmonic oscillators.

In the present paper we explore the escapes in the classical system (1) and a very different problem of escapes, using a system from the domain of General Relativity. In particular the system we use belongs to the so-called Manko-Novikov (MN) metric family. Manko and Novikov (1992) found an exact vacuum solution of Einstein’s equations which describes a stationary, axisymmetric, and asymptotically flat spacetime with arbitrary mass-multipole moments. The MN metric subclass that we use can be considered as a perturbation of the Kerr metric (Kerr 1963) and it was introduced by Gair et al. (2008). The Kerr metric represents a rotating black hole of mass  $M$  and spin  $S$ . The MN perturbation is expressed by a parameter  $q$ , which measures how much the MN quadrupole moment  $Q$  departs from the Kerr quadrupole moment  $Q_{Kerr} = -S^2/M$  (i.e.  $q = (Q_{Kerr} - Q)/M^3$ ). While the Kerr metric describes an integrable system, the MN metric describes a non-integrable system that allows chaos. The line element of the MN metric expressed in the Weyl-Papapetrou cylindrical coordinates  $(\rho, \varphi, z)$  is of the form

$$ds^2 = -f(dt - \omega d\varphi)^2 + f^{-1}[e^{2\gamma}(d\rho^2 + dz^2) + \rho^2 d\varphi^2], \quad (2)$$

where  $f$ ,  $\omega$ ,  $\gamma$  are considered as functions of the prolate spheroidal coordinates  $v, w$ , while the coordinates  $\rho, z$  can be expressed as functions of  $v, w$  as well. Thus

$$\rho = k\sqrt{(v^2 - 1)(1 - w^2)}, \quad z = kvw \quad (3)$$

and

$$f = e^{2\psi} \frac{A}{B}, \quad (4a)$$

$$\omega = 2ke^{-2\psi} \frac{C}{A} - 4k \frac{\alpha}{1-\alpha^2}, \quad (4b)$$

$$e^{2\gamma} = e^{2\gamma'} \frac{A}{(v^2-1)(1-\alpha^2)^2}, \quad (4c)$$

$$A = (v^2-1)(1+ab)^2 - (1-w^2)(b-a)^2, \quad (4d)$$

$$B = [(v+1) + (v-1)ab]^2 + [(1+w)a + (1-w)b]^2, \quad (4e)$$

$$C = (v^2-1)(1+ab)[(b-a) - w(a+b)] \\ + (1-w^2)(b-a)[(1+ab) + v(1-ab)], \quad (4f)$$

$$\psi = \beta \frac{P_2}{R^3}, \quad (4g)$$

$$\gamma' = \ln \sqrt{\frac{v^2-1}{v^2-w^2}} + \frac{3\beta^2}{2R^6} (P_3^2 - P_2^2) \\ + \beta \left( -2 + \sum_{\ell=0}^2 \frac{v-w + (-1)^{2-\ell}(v+w)P_\ell}{R^{\ell+1}} P_\ell \right), \quad (4h)$$

$$a = -\alpha \exp \left[ -2\beta \left( -1 + \sum_{\ell=0}^2 \frac{(v-w)P_\ell}{R^{\ell+1}} \right) \right], \quad (4i)$$

$$b = \alpha \exp \left[ 2\beta \left( 1 + \sum_{\ell=0}^2 \frac{(-1)^{3-\ell}(v+w)P_\ell}{R^{\ell+1}} \right) \right], \quad (4j)$$

$$R = \sqrt{v^2 + w^2 - 1}, \quad (4k)$$

$$P_\ell = P_\ell\left(\frac{v-w}{R}\right). \quad (4l)$$

Here  $P_\ell(\zeta)$  is the Legendre polynomial of order  $l$

$$P_\ell(\zeta) = \frac{1}{2^\ell \ell!} \left( \frac{d}{d\zeta} \right)^\ell (\zeta^2 - 1)^\ell, \quad (5)$$

while the parameters  $k, \alpha, \beta$  are related to the mass  $M$ , the spin  $S$ , and the quadrupole deviation  $q$  through the expressions

$$\alpha = \frac{-1 + \sqrt{1-\chi^2}}{\chi}, \quad k = M \frac{1-\alpha^2}{1+\alpha^2}, \quad \beta = q \left( \frac{1+\alpha^2}{1-\alpha^2} \right)^3. \quad (6)$$

while  $\chi$  is the dimensionless spin parameter  $\chi = S/M^2$ . These formulae give the Kerr metric when  $q = 0$ .

Contrary to the system (1), the escapes in the MN system refer not only to infinity, but also to orbits that fall into the central compact object called ‘‘bumpy black hole’’ by Gair et al. (2008). The MN central compact object is not really a black hole, because its horizon is broken along the equator and regions of closed timelike curves exist outside the horizon (Gair et al. 2008). The MN problem is very different from the simple Hamiltonian (1); however, the two problems have several common properties concerning the role of the periodic orbits and their relations to escapes.

In the present paper we study in detail the periodic orbits in the systems (1) and (2) and their connection with the escape phenomena. We found that the periodic orbits in general do not lead to escapes, except in very special cases. Most of the families of periodic orbits generate an infinity of unstable, but non-escaping, periodic orbits. On the other hand, the asymptotic curves of the various unstable periodic orbits play an important role in generating chaos and most chaotic domains lead to escapes when the energy goes beyond the escape energy.

The paper is organized as follows. In section 2 we calculate the periodic orbits of the system (1). Then we find the asymptotic curves of the unstable periodic orbits and the corresponding chaos. In section 3 we find the escapes from the system (1) and their statistics. In section 4 we find the periodic orbits in the system (2) and the chaotic domains. In section 5 we find the corresponding escapes and their statistics. Finally, in section 6 we compare the two systems and draw our main conclusions.

## 2 Periodic Orbits in the system (1)

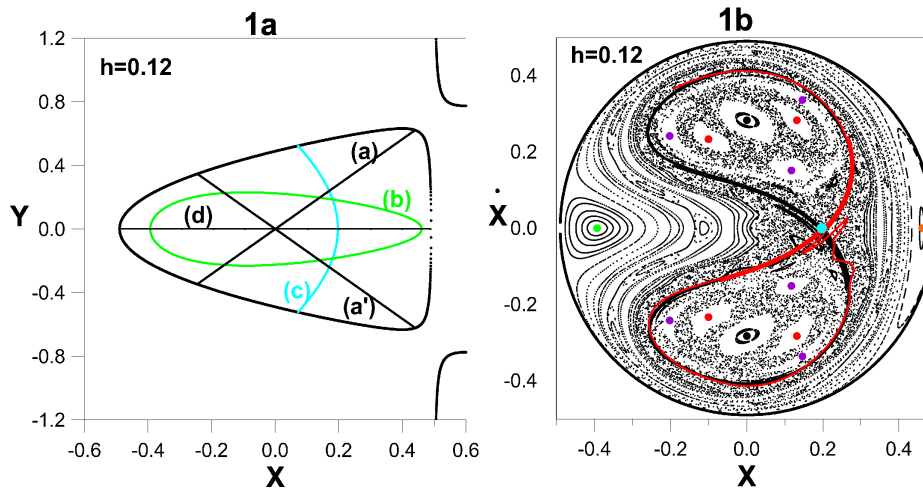


**Fig. 1** (1a) Simple periodic orbits (of period 1) for energy  $h = 0.12$ . (1b) A surface of section  $(x, \dot{x})$  for  $h = 0.12$  containing ordered and chaotic orbits. On the  $\dot{x} = 0$  axis there are two stable periodic orbits (b) and an unstable orbit (c) (at the intersection of the red and black curves), together with one stable (red) and one unstable (thick black) asymptotic manifolds. There are also two stable orbits (a) on the  $x = 0$  axis and triple and double period stable orbits that have bifurcated from the orbits (a) and (a') on the  $x=0$  axis.

For small values of the energy the system (1) has 4 periodic orbits of period 1. There are two straight line periodic orbits

$$y = \pm\sqrt{2} x \quad (7)$$

that are stable (orbits (a) and (a') in Fig. 1a). There is also a stable orbit (b), like an ellipse, described clockwise or counterclockwise, a simple unstable orbit

crossing the  $x$ -axis perpendicularly (orbit (c)), and the orbit  $y = 0$  (orbit (d)). In Fig. 1b we see also 2 stable triple orbits 3 : 1 and 2 stable double orbits 2 : 1 that have bifurcated from the orbits (a) and (a').

The orbits  $y = \pm\sqrt{2}x$  undergo an infinity of transitions to instability and stability as  $h$  tends to  $h_{esc}$  while the period of these orbits tends to infinity (Contopoulos and Zikides 1980). The periodic orbits  $a$  and  $a'$  terminate at  $h = h_{esc}$  when their period is infinite, in accordance with the Strömberg termination principle (Szebehely 1967). For  $h > h_{esc}$  the Curve of Zero Velocity (CZV) ( $x^2 + y^2 - 2x y^2 = 2h$ ) opens and the orbits  $a$  and  $a'$  escape to infinity.

The families (a) and (a') at every transition to stability or instability generate by bifurcation new families of equal or double period. Families of higher order are also bifurcated from the families (a) and (a').

On a surface of section  $(x, \dot{x})$  with ( $y = 0$  and  $\dot{y} > 0$ ) the stable orbits are surrounded by islands of stability, while the unstable orbit is surrounded by a set of chaotic orbits (Fig. 1b). In particular the orbits (a) and (a') appear on the axis  $x = 0$  of Fig. 1b. Near the unstable orbit (c) there is a chaotic region (Fig. 1b).

As  $h$  increases the chaotic region around the unstable orbit (c) increases, while various sets of higher order periodic orbits bifurcate from the straight line orbits ((a), (a')) (Fig. 1b).

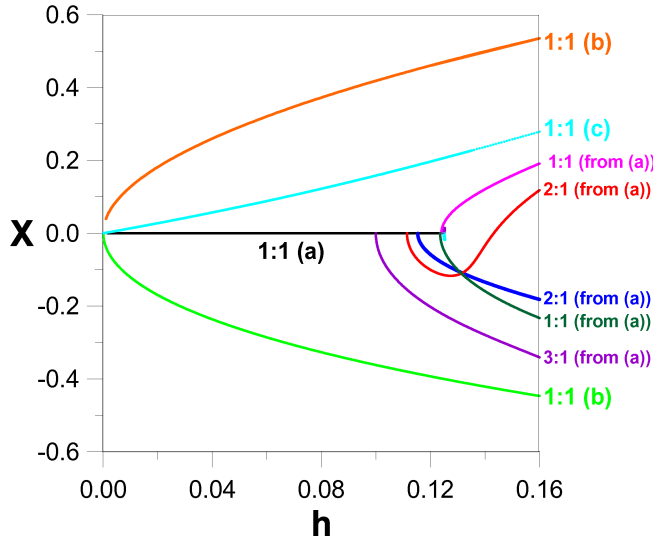


**Fig. 2** Characteristics of some of the most simple families of periodic orbits. The family (a) and its bifurcations have  $\dot{x} \neq 0$

The characteristics of the various families of periodic orbits are shown in Fig. 2. These characteristics give the value of  $x$  when  $y = 0$  and  $\dot{y} > 0$ . We mark in particular the orbits 3 : 1, 2 : 1 and 1 : 1 bifurcating from the orbits (a) and (a') as the energy  $h$  increases. The stability of these families is given in Fig. 3. The orbits are stable if their Hénon parameter  $a$  is between  $-1$  and  $+1$ .

The family  $y = \sqrt{2} x$  (a) is stable for  $0 < h < 0.111$ , then unstable in the interval  $0.111 < h < 0.116$ , stable again for  $0.116 < h < 0.1236$ , and has infinite

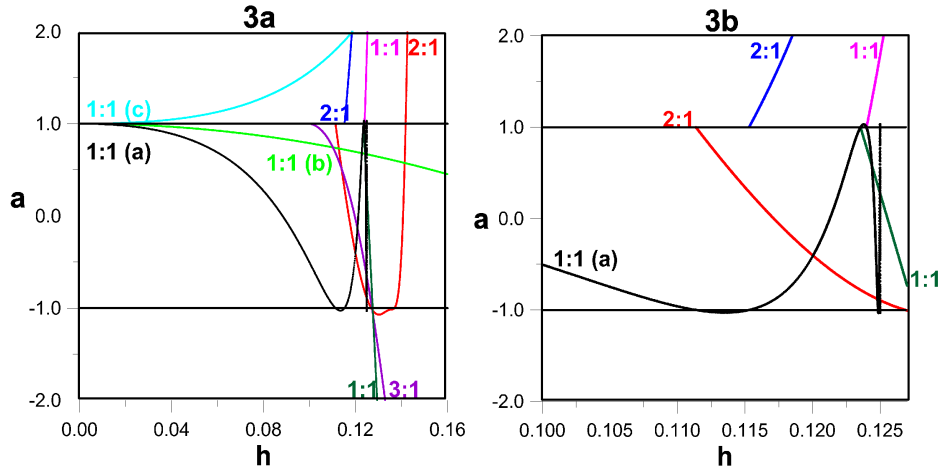


**Fig. 3** (3a) The Hénon stability parameter  $a$  of the families of Fig. 2 as a function of the energy  $h$ ; (3b) Details of Fig. 3a.

more transitions to instability and stability until  $h = h_{esc} = 0.125$ . At the first transition to instability ( $h = 0.111$ ) the value of  $a$  goes below  $a = -1$  and one stable family of double period bifurcates there. Its stability is represented by the red curve in Fig. 3, starting at  $a = 1$ .

At the first transition from instability to stability along the family (a) ( $h = 0.116$ )  $a$  goes above  $a = -1$  and there is a bifurcation of an unstable family  $2 : 1$  (blue curve above  $a = 1$ ).

At the second transition to instability the value of  $a$  goes above  $a = 1$  ( $h = 0.1236$ ) and two different stable families of equal period bifurcate there (black  $1:1$ ). The orbits of these families deviate from the straight line  $y = \sqrt{2} x$ . At the second transition to stability there are bifurcations of two unstable families (magenta  $1:1$ ), and so on.

Symmetric bifurcations are formed also around the family ( $a'$ ). There are also higher order bifurcations from the families ( $a$ ) and ( $a'$ ), e.g. the family  $3 : 1$  (Figs. 2 and 3a).

The families bifurcating from the orbit (a) consist of orbits that reach the CZV at two points. These families do not terminate for  $h$  larger than  $h = 0.125$ , but extend all the way to  $h = \infty$ . An example of an orbit of such a family ( $2 : 1$ ) is shown in Fig. 4a for  $h = 0.2$ . This family is bifurcated from the family (a) for  $h = 0.111$  and it is stable in the interval  $0.111 < h < 0.1252$ . At  $h = 0.1252$  the family  $2 : 1$  becomes unstable and generates a family with double period (i.e. 4 times the original period). For  $h = 0.137$  the family  $2 : 1$  crosses again the  $a = -1$  axis (Fig. 3a) and becomes again stable generating an unstable double period family (i.e. 4 times the original period). Finally, at  $h = 0.142$  the family  $2 : 1$  crosses the  $a = 1$  axis and becomes unstable for larger  $h$ . At this crossing point it generates an equal period stable family (2 times the original period). This also becomes unstable for a slightly larger  $h$ , followed by a cascade of period doubling bifurcations, that generate an infinity of unstable families, that exist for arbitrarily large  $h$ .

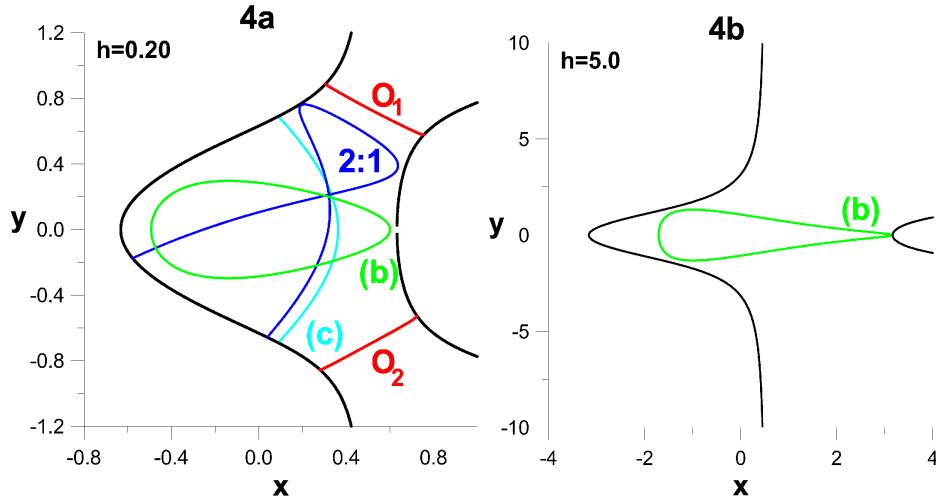


**Fig. 4** (4a) Some periodic orbits for  $h = 0.2$ . Four periodic orbits of period 1, (b), (c), and the Lyapunov orbits  $O_1$ ,  $O_2$ , and a periodic orbit of period 2, belonging to the family bifurcating from the family (a). (4b) An (unstable) periodic orbit (b) for  $h = 5.0$ .

When  $h > h_{esc} = 0.125$  the CZVs open above and below the axis ( $y = 0$ ) (Fig. 4a,b) and several orbits escape to infinity. However, the periodic orbits of Figs. 4a,b do not escape. E.g. the orbit 2 : 1 in Fig. 4a that bifurcated from the orbit (a) at  $h = 0.111$  does not escape, although the orbit (a) has escaped. In Fig. 4b we show a non-escaping orbit (b) for  $h = 5.0$  when the openings are very large.

At every opening of the CZV there is an unstable orbit (called Lyapunov orbit) crossing it (Fig. 4a). Any orbit, crossing a Lyapunov orbit outwards, escapes to infinity (Churchill et al. 1975; Contopoulos and Efsthathiou 2004). The regions of direct escape are shown in red in Fig. 5 for  $h = 0.132$ . Orbits starting in these regions escape directly, without any intersections with the axis  $y = 0$ . The boundaries of the direct escape regions are defined by the asymptotic curves of the Lyapunov orbits. These asymptotic curves make infinite rotations around the escape regions (Contopoulos 1990). In that paper we described in detail the asymptotic curves from the Lyapunov orbits. We found that these asymptotic curves include an infinity of branches that start and end with infinite rotations around the escape regions. The stable asymptotic curves of any other unstable periodic orbit leading to escapes approach the same limiting asymptotic curves, i.e. the boundaries of the red regions as in Fig. 5. For relatively small values of the energy  $h$ , however, most of the chaotic orbits escape after one or more intersections with the axis  $y = 0$  (Fig. 5).

The asymptotic curves of the unstable orbit (c) surround the red escape regions. Examples of such asymptotic curves are shown in Figs. 1b and 5. The unstable asymptotic curves start in opposite directions and the stable asymptotic curves start also in opposite directions. In Figs. 1b and 5 we give in black the unstable asymptotic curve that starts towards the right downwards and surrounds clockwise the lower red region. As it comes again close to the point (c) it makes several oscillations, up and down close to the point (c).

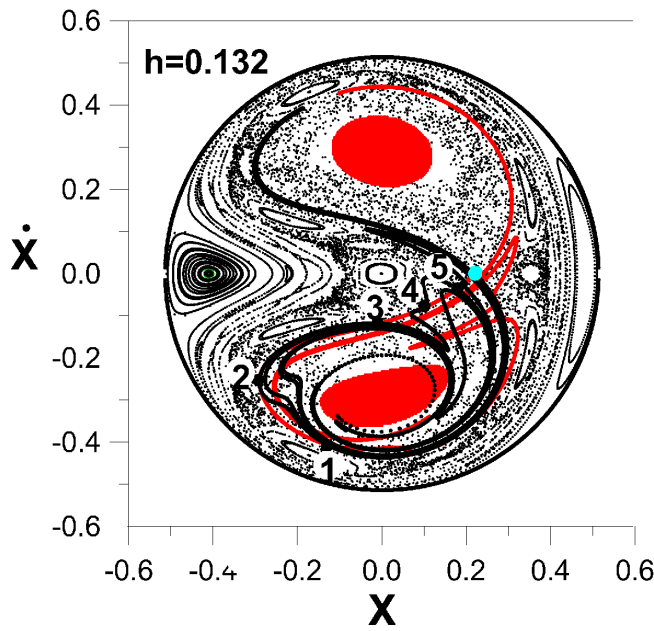


**Fig. 5** Surface of section for  $h = 0.132$ . The orbits in the red regions escape directly to infinity without any intersection with the axis  $y = 0$ . Blue dot corresponds to the orbit (c).

The stable asymptotic curve (red) starts to the left and downwards, surrounding counterclockwise the red escape region and intersects the unstable asymptotic curve at several homoclinic points. The oscillations of the stable and unstable asymptotic curves are much larger in Fig. 5 ( $h = 0.132$ ) than in Fig. 1b ( $h = 0.12$ ). But the main difference between Figs. 1b and 5 is that in the first case there are no escapes, while in the second case most of the chaotic orbits escape to infinity. The orbits that escape directly without any intersection with the axis  $y = 0$ , are marked in red. The stable asymptotic curve (red curve) of the unstable periodic orbit (c) (blue dot in Fig. 5) makes an infinity of rotations around the lower red region. This asymptotic curve never intersects the red regions. This happens because orbits starting on the stable asymptotic curve have further intersections along the same asymptotic curve, until they reach asymptotically the periodic orbit. Therefore they cannot escape immediately, hence they cannot be found inside a red region.

On the other hand, the unstable asymptotic curve (black curve) intersects the red region after a number of oscillations below and above the stable asymptotic curve (Fig. 5). The stable and unstable asymptotic curves intersect at an infinity of homoclinic points. A few points (1 – 5) are marked in Fig. 5. The corresponding homoclinic orbits approach asymptotically the periodic orbit (c) as  $t \rightarrow \infty$  and  $t \rightarrow -\infty$ . The unstable asymptotic curve (black) makes outer and inner loops above and below the stable asymptotic curve. The areas of these lobes are equal. The homoclinic intersections approach closer and closer the periodic orbit (c), their distances decreasing proportionally to  $1/\lambda$ , where  $\lambda$  is the larger (positive) eigen-

value of the orbit (c). Thus the lengths of the lobes become longer proportionally to  $\lambda$ . The value of  $\lambda$  increases as the energy increases.

The inner lower lobes make some rotations, back and forth, around the lower red escape region. The inner loop starting downwards from the homoclinic point 5 makes 1/2 rotation around the red region and returns closer than the point 5 to the periodic orbit (c). The next inner loop makes about 1.5 rotations around the red region and the subsequent loop intersects the red region (Fig. 5).

Then the orbits passing through points of the black curve inside the red region, escape to infinity without any further intersections with the surface of section. As a point along the black curve approaches the red region its next image on the surface of section makes an infinity of rotations around the upper red region of Fig. 5 approaching asymptotically the boundary of the red region. This phenomenon is described in detail in the paper of Contopoulos and Efsthathiou (2004).

For values of  $h$  up to about 0.32 there are some stable families, generated from the stable family (b), of orbits starting on the  $y = 0$  axis. This family consists of almost elliptical orbits that are described either clockwise or counterclockwise (Figs. 1a,b). The family (b) is stable up to about  $h = 0.304$  and then it becomes unstable at a period doubling bifurcation ( $a = -1$ ). The double period families bifurcating from (b) start at  $a = +1$  and become unstable at another period doubling bifurcation (4 times the original period) for about  $h = 0.32$ . Thus the interval between the first and the second period doubling bifurcations is  $\Delta h = 0.016$ . This is followed by a cascade of period doubling bifurcations that produce an infinity of unstable families, existing for arbitrarily large  $h$ . It is known that the intervals between successive period doubling bifurcations in conservative systems decrease by a universal (asymptotic) factor  $\delta = \frac{1}{8.2}$  (Eckmann 1981). Therefore, the total interval  $\Delta h$  that contains higher order bifurcation of the family (b) is approximately  $\Delta = \frac{0.016}{1 - \frac{1}{8.2}} = 0.018$ , and beyond  $h = 0.304 + 0.018 = 0.322$  there is no stable periodic orbit generated by bifurcations from the family (b).

When the orbit (b) has just become unstable there are two islands of stability around it. For  $h = 0.305$  (Fig. 6) the asymptotic curves of the orbit (b) surround the two islands, but they do not extend to large distances. In fact, for this value of  $h$  there are invariant curves surrounding the orbit (b) and the islands around it. However, for still larger  $h$  the asymptotic curves of (b) extend very far (Fig. 7a) surrounding the whole available area on the surface of section (Fig. 7b). The invariant curves surrounding the point (b) for  $h = 0.305$ , have been destroyed for  $h = 0.31$  and the asymptotic curves come close to the limiting curve  $\dot{x}^2 + x^2 = 2h$ .

The same pattern of transition to instability is followed by most stable periodic orbits. Namely most stable orbits become unstable at a period doubling bifurcation followed by a cascade of infinite period doublings that lead to an infinity of unstable periodic orbits. An exception are the families (a) (a'), which have a non-universal bifurcation ratio  $\delta = 9.22$  and lead to escapes (Contopoulos and Zikides 1980). A theoretical explanation of this particular bifurcation ratio was provided by Heggie (1983). A review of previous theoretical and numerical work on bifurcations is provided by Contopoulos (2002).

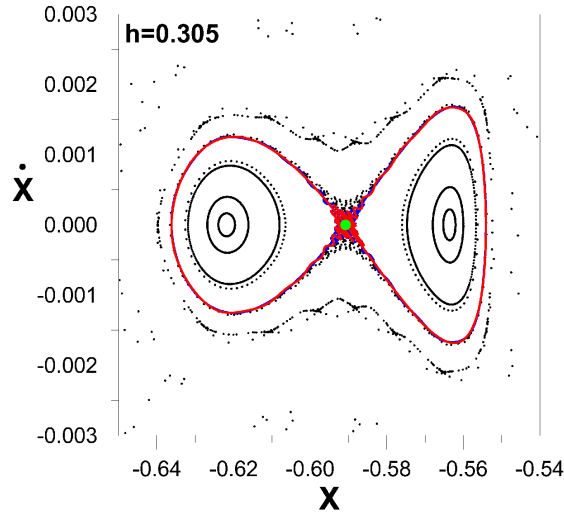


**Fig. 6** The periodic orbit ( $b$ ) on the surface of section for  $h = 0.305$ , when the periodic orbit has just become unstable, and two stable orbits that bifurcated from it. The asymptotic curves from the orbit ( $b$ ) surround both islands of stability, but they do not extend to larger distances.

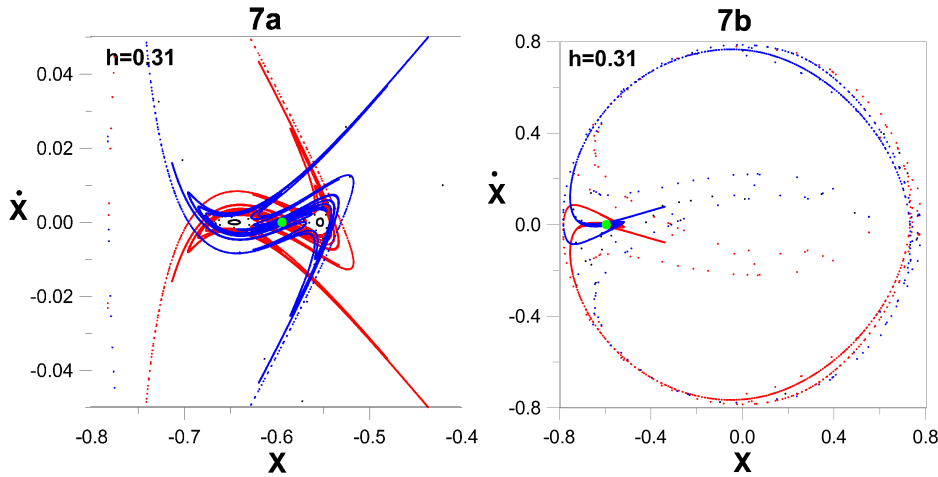


**Fig. 7** The asymptotic curves (blue=unstable and red=stable) of the orbit ( $b$ ) for  $h = 0.31$  extend well beyond the areas around the two islands (Fig. 7a) and go all around the available area on the surface of section (Fig. 7b).

### 3 Escapes from the system (1)

As the energy  $h$  increases the proportion of orbits, that escape directly through the openings of the the CZV increases. In Fig. 5 ( $h = 0.132$ ) the upper red region represents orbits that escape through the upper opening of the CZV, and the lower red region represents orbits that escape through the lower opening of the CZV, without ever intersecting the axis  $y = 0$ . However, most of the chaotic orbits,

represented by scattered dots in Fig. 5, escape from the system after a small or large number of intersections with the  $y = 0$  axis.

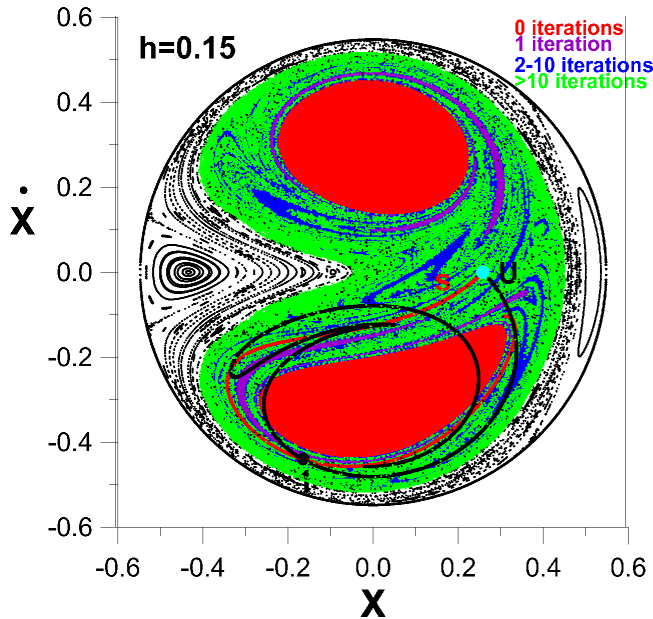
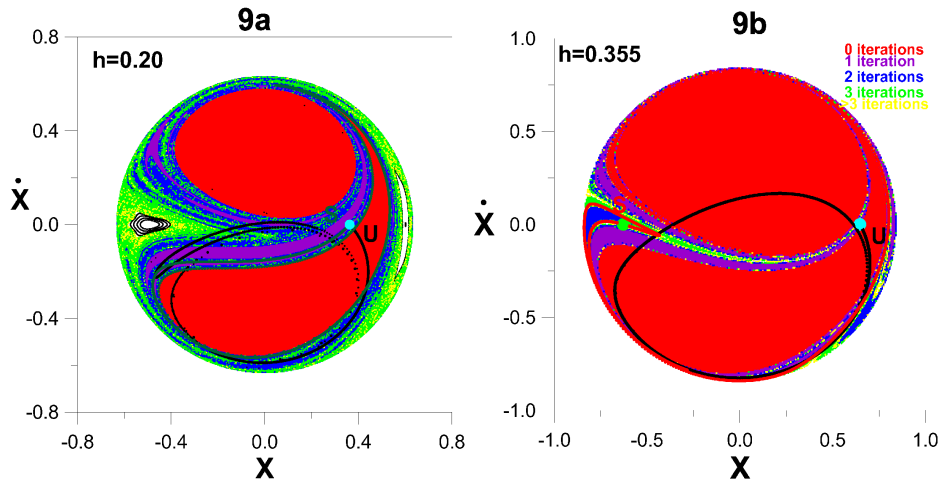


Fig. 8 Escape regions for  $h = 0.15$ .

As  $h$  increases to  $h = 0.15$  the red regions increase in relative size (proportion of the total area). In Fig. 8 are shown the direct escape regions for  $h = 0.15$  and the asymptotic curves (black, unstable and red, stable), from the periodic orbit (c), in the lower part of the figure. The regions in Fig. 8 are colored according to the number of intersections an orbit has with the axis  $y = 0$  before the orbit escapes. The stable asymptotic curve (red) again does not intersect the red region, but the (black) unstable asymptotic curve intersects the red region on the left after half a rotation around it. Then it intersects it again (after an inner and an outer loop, below and above the stable asymptotic curve) on the right side of the red region and so on. The orbits starting at points of the black curve inside the red region escape again without any further intersections with the axis  $y = 0$ .

For larger  $h$  ( $h = 0.20$ ) (Fig. 9a) and  $h = 0.355$  (Fig. 9b) the two regions of direct escapes increase in proportion to the total available space.

In Fig. 9b we have marked one unstable asymptotic curve of the unstable periodic orbit (c) (black), and one stable asymptotic curve of the unstable periodic orbit (b) on the left (red). The two curves are almost tangent at a point. We have checked that for  $h = 0.354$  the two asymptotic curves do not intersect and for  $h = 0.356$  they clearly intersect close to this point. Thus, for a value of  $h$  a little smaller than  $h = 0.355$  the two curves are tangent. Then according to the Newhouse theorem (1977; 1983) close to the tangency point there is a stable periodic orbit, generated at a tangent bifurcation.



**Fig. 9** (9a) Escape regions for  $h = 0.25$  either directly (red), or after a number of intersections of the  $y = 0$  axis upwards ( $\dot{y} > 0$ ), as indicated in the color scale. The white region represents an island of stability. We mark also an unstable asymptotic curve ( $U$ ) from the periodic orbit ( $c$ ). (9b) The same, as in Fig. 9a, for  $h = 0.355$ , together with an initial arc of the stable asymptotic curve of the orbit ( $b$ ) on the left (red).

In Figs. 9a,b we see that the periodic orbits ( $b$ ) and ( $c$ ) are in a region where escapes occur after several intersections of the axis  $y = 0$  by the orbits. In fact, the periodic orbits never escape, and orbits close to them escape after a time that increases to infinity as the initial conditions approach the periodic orbits. In particular the stable asymptotic curves do not intersect the red regions of direct escapes. In fact, all the orbits starting on the stable asymptotic curves never escape.

On the other hand, the unstable asymptotic curve  $U$  of ( $c$ ) in Figs. 9a,b enters the red region at a rather small distance from the orbit ( $c$ ), and the orbits starting inside the red region escape directly. However, this unstable asymptotic curve comes out of the red region several times, hence the corresponding orbits escape in general after some intersections with the axis  $y=0$ .

The fact that there are chaotic orbits that escape after long times is related to the phenomenon of stickiness along the unstable asymptotic curves (Contopoulos and Harsoula 2008, 2010).

As  $h$  increases further new tangencies between the unstable and the stable asymptotic curves of the unstable orbits are formed, thus new stable periodic orbits appear. However, the islands around these periodic orbits are extremely small, since almost 100% of the orbits escape for large  $h$ .

This situation is similar to the case where no escapes exist at all, but tangencies between the asymptotic curves generate new stable periodic orbits (Contopoulos et al. 1994).

We proceed now to a statistical analysis of the escapes. This is done in four ways:

- (a) First we separate the orbits into ordered and chaotic + escaping. In Fig. 10a we give the proportion of the chaotic orbits  $N_{cha}/N_o$  (including the escaping orbits) as a function of the energy  $h$ . Namely we populate the whole circle inside

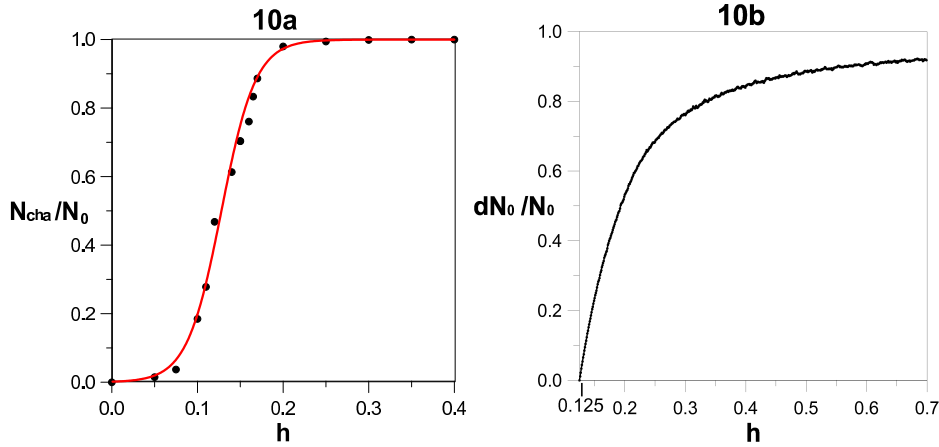


**Fig. 10** (10a) The proportion of chaotic (including escaping) orbits  $N_{cha}/N_0$  as a function of the energy  $h$ . (10b) The proportion of the directly escaping orbits  $dN_0/N_0$  (without any intersection with the axis  $y = 0$ ) as a function of the energy  $h$ .

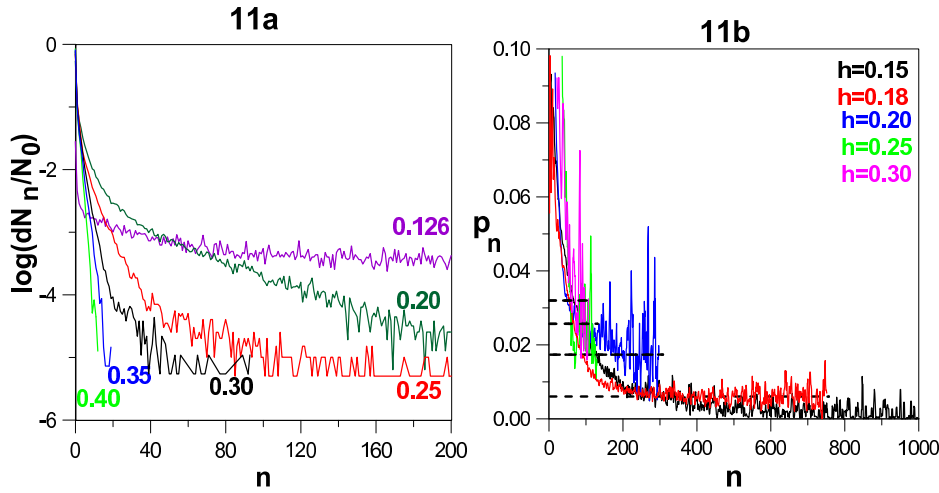


**Fig. 11** (11a) The logarithmic proportions  $\log(\frac{dN_n}{N_0})$  of escapes for  $h = 0.126, 0.20, 0.25, 0.30, 0.35$  and  $0.40$  as functions of the number of intersections  $n$ . (11b) The probability  $p_n = \frac{dN_n}{N_n}$  of escapes as a function of  $n$  for various values of the energy  $h$ .

the limiting curve  $x^2 + \dot{x}^2 = 2h$  by initial conditions of  $N_0$  orbits (where  $N_0 = \pi(250)^2 \simeq 200000$ ) and we find the total numbers of chaotic + escaping orbits  $N_{cha}$ . Then the number of ordered orbits is  $N_0 - N_{cha}$ . When  $h$  is very small the proportion of ordered orbits is almost 100%. As  $h$  increases the proportion of chaotic orbits increases and for  $h = 0.125$  this proportion is about 50% (Fig. 10a). When  $h$  goes beyond the escape perturbation  $h = 0.125$  the proportion of chaotic orbits increases, but most chaotic orbits escape to infinity. Only a very small proportion of chaotic orbits near higher order unstable periodic

orbits inside islands of stability do not escape (like the orbits near the unstable periodic orbit (b) of Fig. 6).

The proportion of chaotic orbits (including the escaping orbits) can be given by the approximate formula (Fig. 10a)

$$N_{cha}/N_0 = 0.5[1 + \tanh(30.0h - 4.0)]. \quad (8)$$

For small  $h$  this proportion tends to zero, while for large  $h$  it tends to 1.

- (b) We calculate the proportion of direct escapes (Fig. 10b),  $dN_o/N_o$  (where  $dN_o$  is the number of orbits that escape without any intersection with the axis  $y = 0$ ) as a function of the energy  $h$ . The direct escape regions are red in Figs. 5, 8, 9a,b. This proportion is small for  $h$  slightly larger than  $h_{esc} = 0.125$  and increases fast with  $h$ , reaching more than 90% for  $h = 0.7$ .
- (c) Then we study the escape time. The time is represented by the number of intersections  $n$  before escape. Most escapes take a long time for  $h$  slightly above  $h_{esc}$  and take place faster as  $h$  increases. In Fig. 11a we give the logarithm of the proportion of escaping orbits  $dN_n/N_0$  where  $dN_n$  is the number of escapes after the  $n$ th intersection (upwards,  $\dot{y} > 0$ ) and before the  $(n + 1)$  intersection (i.e. there is no  $(n + 1)$  intersection). We see that the escape rates are decreasing with  $n$ . The escape rates  $dN_n/N_0$  are large for small  $n$  and decrease considerably for larger  $n$ . For  $h \geq 0.35$  the escapes take place quite fast.
- (d) Finally, we calculate the probability of escape as a function of time represented by the number of intersections  $n$  for various values of the energy. Namely the probability  $p_n$  is the ratio  $dN_n/N_n$  where  $N_n$  is the number of orbits that have not yet escaped before the  $n$ th intersection

$$p_n = \frac{dN_n}{N_n}. \quad (9)$$

This probability was calculated for the system (1) and other similar systems in previous papers (Contopoulos et al. 1993; Siopis et al. 1995a,b, 1996). It was found that  $p_n$  tends to a constant value  $p$ , independent of the initial conditions of non-ordered orbits. For large times (large  $n$ ) the probability of escape tends to zero if the energy is smaller than a critical value  $h_{cr}$ , larger than the escape energy  $h_{esc}$ . However, if  $h$  is larger than  $h_{cr}$ , the probability  $p_n$  for large  $n$ , tends to a constant value  $p$  larger than zero. This quantity depends only on the energy  $h$ . In our present notation the limiting probability  $p$  is proportional to a power of the quantity  $(h - h_{cr})$ , i.e.

$$p \propto (h - h_{cr})^\alpha, \quad (10)$$

where  $h_{cr}$  is the critical value of  $h$ , and the exponent  $\alpha$  is approximately  $\alpha = 0.5$ . This value of  $\alpha$  was found to be the same for different dynamical systems (Siopis et al. 1995a,b).

In Fig. 11b we give the value of  $p_n$  as a function of  $n$  for various values of  $h$ . When  $h = 0.15$  the probability  $p_n$  tends to  $p = 0$ . On the other hand when  $h = 0.18, 0.20, 0.25, 0.30$  the probabilities tend to  $p = 0.006, 0.018, 0.026, 0.034$ . These values can be approximated by the formula

$$p = 0.11(h - h_{cr})^{0.53}. \quad (11)$$

where  $h_{cr} = 0.175$ . This formula is consistent with the universal formula found by Siopis et al. (1995a,b).

The statistics of escapes in various dynamical systems has been a subject of considerable interest in recent years. The main question is whether the various chaotic phenomena (like Poincaré recurrences, correlations and escapes) decay exponentially in time or according to power laws (e.g. Cristadoro and Ketzmerick 2008; Venegeroles 2009). The power laws are supposed to be connected to the existence of stickiness in mixed dynamical systems that contain islands of stability. However a detailed study of the effects of stickiness on the escapes should be the study of a future research.

#### 4 Periodic Orbits in the Manko-Novikov metric (2)

The Manko-Novikov (MN) spacetime depends on a parameter  $q$  that measures the quadrupole moment deviation of this metric from the Kerr metric with the same mass  $M$  and spin  $S$ . There have been proposals and attempts to constrain such deviations from observational data (see e.g. Psaltis and Johannsen (2010); Bambi (2011); Bambi and Barausse (2011a,b) and references therein). The final stages before the plunge (escape) in a non-Kerr spacetime like the MN have certain astronomical interest (see Bambi and Barausse (2011b)). From this point of view our work aims to exploit the non-integrability of the MN metric in order to give a detailed example of a such a final stage.

The geodesic orbits of a test particle of mass  $\mu$  are described as equations of motion of the following Lagrangian

$$L = \frac{1}{2} \mu g_{\mu\nu} \dot{x}^\mu \dot{x}^\nu. \quad (12)$$

The MN metric has two integrals of motion (Gair et al. 2008; Lukes-Gerakopoulos et al. 2010), namely the energy (per unit mass)

$$E = -\frac{\partial L}{\partial t} / \mu = f(\dot{\gamma} - \omega \dot{\varphi}), \quad (13)$$

and the z-component of the angular momentum (per unit mass)

$$L_z = \frac{\partial L}{\partial \dot{\varphi}} / \mu = f\omega(\dot{t} - \omega \dot{\varphi}) + f^{-1} \rho^2 \dot{\varphi}, \quad (14)$$

where the dots mean derivatives with respect to the proper time. The Kerr metric has one more integral of motion, the so-called Carter constant (Carter 1968), thus it is an integrable system. However, the MN model is non-integrable and it allows the appearance of chaos.

The motion on a meridian axis ( $\varphi = \text{const}$ ) in the MN system satisfies the relation

$$\frac{1}{2}(\dot{\rho}^2 + \dot{z}^2) + V_{eff}(\rho, z) = 0, \quad (15)$$

where the effective potential  $V_{eff}(\rho, z)$  depends on  $q$ ,  $E$  and  $L_z$ . Thus the motion takes place inside the CZV

$$V_{eff} \equiv \frac{1}{2} e^{-2\gamma} \left[ f - E^2 + \left( \frac{f}{\rho} (L_z - \omega E) \right)^2 \right] = 0. \quad (16)$$

Studies of the orbits in the MN metric were made by Gair et al. (2008); Apostolatos et al. (2009); Lukes-Gerakopoulos et al. (2010); Contopoulos et al. (2011). In the present paper we study on detail the periodic orbits, chaos and escapes in this system.

In the following we use the values  $q = 0.95$ ,  $M = 1$  and  $\chi = S/M^2 = 0.9$  for the spin. We find the orbits for a fixed value of the  $z$ -angular momentum  $L_z = 3$ , and various values of  $E$ .

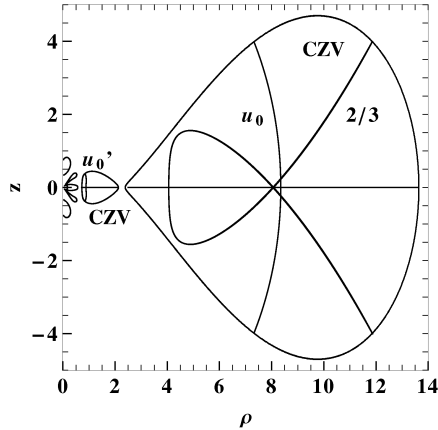


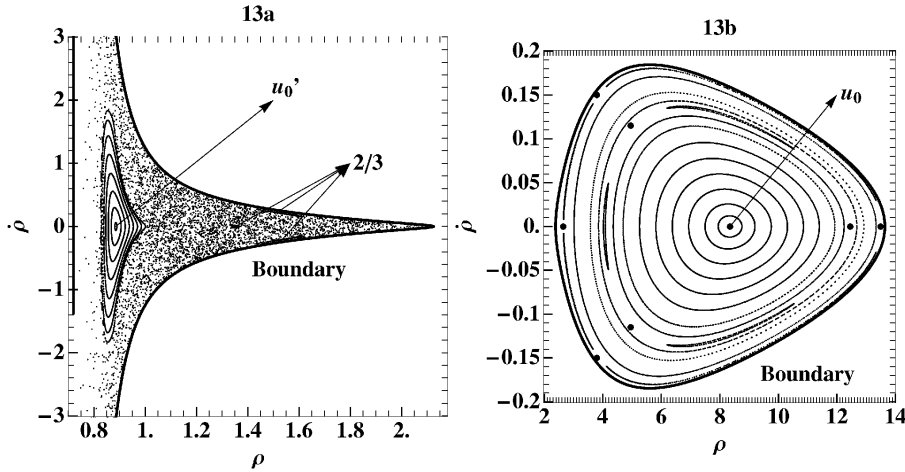
**Fig. 12** Three stable periodic orbits inside the outer CZV:  $u_0$ ,  $2/3$  and  $z = 0$  and two periodic orbits inside the inner CZV  $u'_0$  (stable) and  $z = 0$  (unstable). There are also 5 CZVs that reach the axis  $\rho = 0$ . The line segment  $-0.43589 \leq z \leq 0.43589$  on the axis  $\rho = 0$  represents the horizon of the bumpy black hole. The horizon is broken at the point  $\rho = z = 0$ .

The form of the CZV in the case  $E = 0.95$  is given in Fig. 12. It consists of two main closed curves and 5 more curves of small extent reaching the axis  $\rho = 0$ . The line segment  $-k \leq z \leq k$  ( $k = 0.43589$  for  $M = 1$ ,  $\chi = 0.9$ ), along the axis  $\rho = 0$ , represents the horizon and any orbit reaching this axis escapes into the bumpy black hole. All orbits inside the 5 curves that are close to the horizon escape into the bumpy black hole.

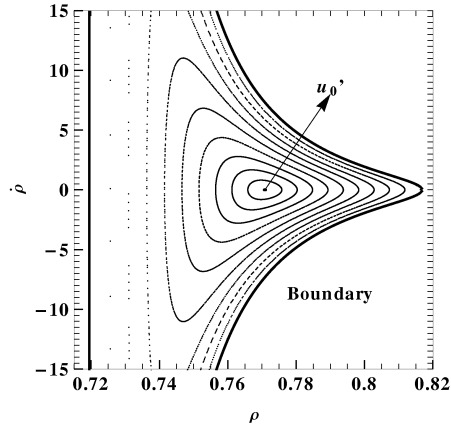
On the other hand, the orbits starting inside the main closed CZVs remain inside these curves for ever. In particular there are two simple periodic orbits inside the outer CZV, and two more simple periodic orbits inside the inner CZV. The periodic orbits  $u_0$  (outer) and  $u'_0$  (inner) intersect perpendicularly the  $\rho$ -axis while the other two periodic orbits are straight lines along the  $z = 0$  axis. Furthermore, we mark a stable resonant orbit  $2/3$ . The orbits  $u_0$ ,  $u'_0$  and the outer  $z = 0$  orbit are stable, while the inner  $z = 0$  is unstable.

If we take a surface of section  $(\rho, \dot{\rho})$  the intersections ( $z = 0, \dot{z} > 0$ ) of most orbits inside the outer CZV are along closed invariant curves around the point  $u_0$  that represents the periodic orbit  $u_0$  (Fig. 13b). However, there are also islands of stability around the stable (resonant) periodic orbits, and some chaos between these islands, around the unstable periodic orbits (Fig. 13b).

On the other hand, most orbits in the inner region (inside the inner CZV) are chaotic (Fig. 13a) although there is a large island of stability and three small islands of type  $2/3$ . The chaotic character of these orbits is related to the instability



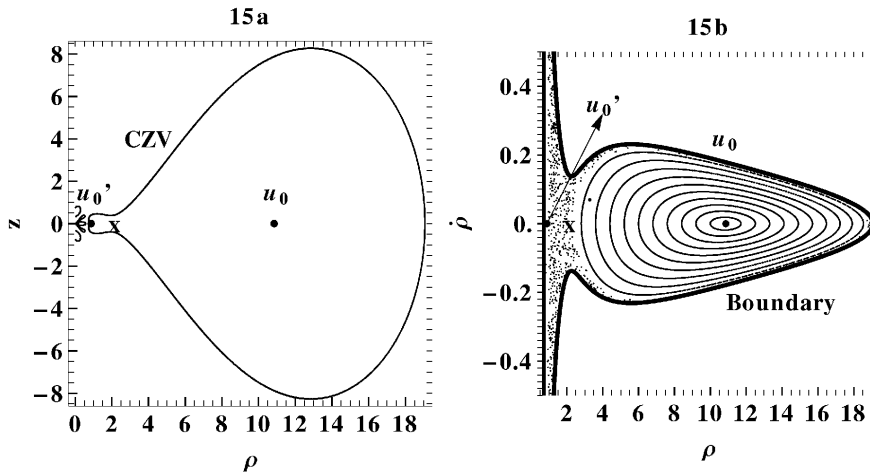
**Fig. 13** Invariant curves and islands on a surface of section  $(\rho, \dot{\rho})$  ( $z = 0$ ) for  $E = 0.95$ . (13a) Islands and chaos in the inner region. (13b) Invariant curves and islands in the outer region. The unstable periodic orbits are marked with big dots.



**Fig. 14** Invariant curves around the periodic orbit  $u_0'$  for  $E = 0.50$ . The boundary represents the orbit  $z = 0$ , which is stable in this case.

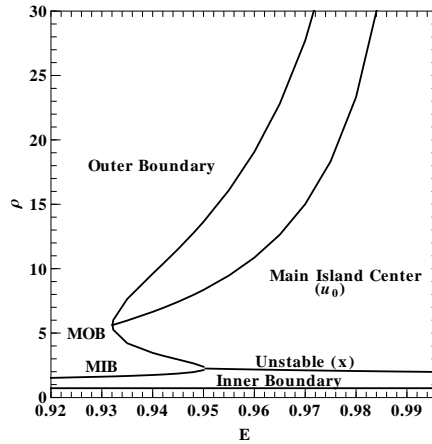
of the orbit  $z = 0$ , which is represented by the boundary of the inner region on the surface of section. However, for a large range of values of  $E$  smaller than  $E = 0.67$  the orbit  $z = 0$  is stable and most orbits around  $u_0'$  are ordered (e.g. for  $E = 0.5$ , Fig. 14).

If  $E$  increases beyond  $E = 0.9504$  the inner and outer CZVs are joined into a common CZV (Fig. 15a for  $E = 0.96$ ). When the two curves join, an unstable periodic orbit is formed, which intersects perpendicularly the  $z = 0$  axis (point x in Fig. 15a) and exists for larger values of  $E$ . At the same time the two periodic orbits  $z = 0$  join into one unstable orbit. The inner and outer regions are also joined on the surface of section  $(\rho, \dot{\rho})$  (Fig. 15b). The periodic orbit  $z = 0$  is represented now



**Fig. 15** (15a) The two main CZV are joined into one for  $E = 0.96$ . The point  $x$  represents an unstable orbit that is generated at the saddle point when the two curves join. (15b) The corresponding surface of section  $(\rho, \dot{\rho})$ . In this case the boundary, which represents the orbit  $z = 0$ , is unstable. Chaos is dominant in the inner region and close to the boundary.

by the common boundary of the two regions and close to it there is some chaos extending all the way around the orbit  $u_0$ . Chaos is also dominant inside (i.e. on the left of) the orbit  $x$  (Fig. 15b).



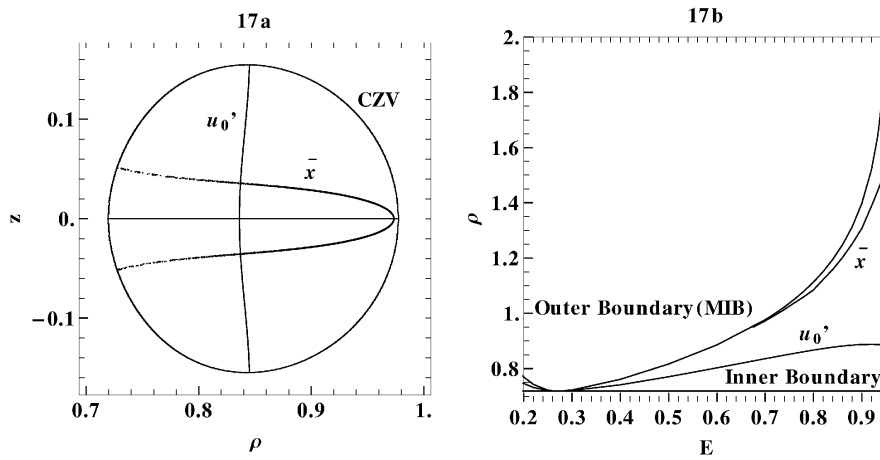
**Fig. 16** Characteristics of the periodic orbits  $(u_0, x)$  and the boundaries of the main permissible regions ( $\rho$  is given as a function of the energy  $E$ ).

Figure 16 gives the characteristics of the periodic orbits  $u_0$  and  $x$  and the boundaries of the permitted motions for  $z = \dot{\rho} = 0$ . The inner boundary is at an almost constant  $\rho \simeq 0.72$ . The outer boundary increases considerably with increasing  $E$  and tends to infinity as  $E \rightarrow 1$ . When  $E > 1$  the orbits escape to

infinity. When  $E < 0.9504$  the permissible region splits into two and we have a middle outer boundary (MOB) (Fig. 16) which is the inner boundary of the outer region, and a middle inner boundary (MIB) which is the outer boundary of the inner region.

As  $E$  decreases the outer region shrinks, and disappears for  $E \simeq 0.9321$ . Then the orbit  $u_0$  also disappears after becoming just one point. Then the orbit in 3 dimensions is a circle on the equatorial axis around the center  $\rho = 0$ . For smaller  $E$  only the inner closed CZV persists.

The position of the orbit  $u'_0$  is close to the inner boundary, and cannot be distinguished from the inner boundary in the scale of Fig. 16. In fact, the distance of this orbit from the inner boundary decreases, as  $E$  decreases, and goes to zero at about  $E = 0.28$  (Fig. 17b). For the same value of  $E$  the outer boundary of the inner region (MIB) reaches the inner boundary. Then the orbit  $u'_0$  in 3 dimensions is circular on the equatorial plane.



**Fig. 17** (17a) Periodic orbits  $u'_0$  and  $\bar{x}$  for  $E = 0.7$ . The family  $\bar{x}$  was generated at the transition of the orbit  $z = 0$  from stability to instability as  $E$  increases. (17b) The characteristics of the families  $u'_0, \bar{x}$  and the boundaries of the (inner) permissible region.

As we have mentioned above the orbit  $z = 0$  of the inner region becomes stable when  $E$  decreases below  $E \simeq 0.67$ . As  $E$  increases above this critical value, a stable family  $\bar{x}$  that crosses perpendicularly the  $z = 0$  axis bifurcates from  $z = 0$  (Fig. 17a,b). As  $E$  increases further this family becomes unstable, generating by bifurcation higher order periodic orbits. E.g. for  $E = 0.95$  one can see 3 small islands around this unstable family (on the right hand side of Fig. 13a).

When  $E$  decreases below  $E = 0.28$  the inner CZV increases again (left side of Fig. 17b), and the orbit  $u'_0$  deviates from the inner boundary. But, for  $E < 0.198$  the distance of  $u'_0$  from the inner boundary decreases again (Fig. 18), although it does not tend to zero.

The most strange evolution occurs when  $E$  becomes smaller than  $E = 0.19236$ . Then a couple of simple periodic orbits crossing perpendicularly the  $z = 0$  axis is

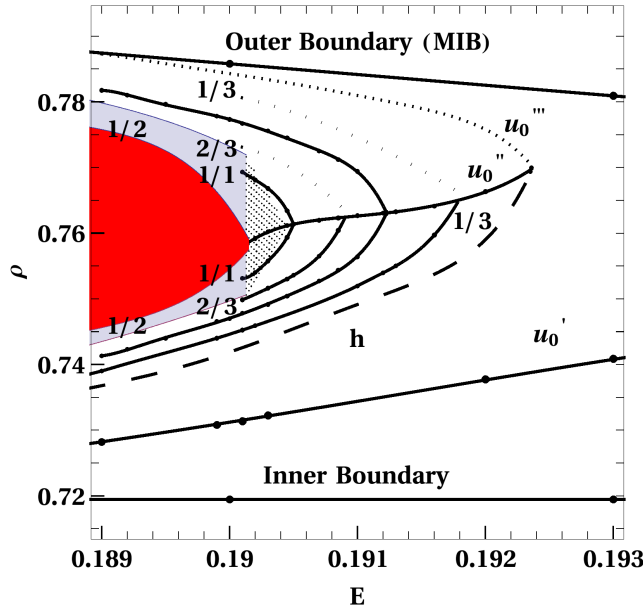


**Fig. 18** Characteristics of the families  $u_0'$ ,  $u_0''$ ,  $u_0'''$  and of some resonant bifurcations from the family  $u_0''$  for relatively small values of the energy  $E$ . The dotted region indicates chaos. The dashed line gives the position of the first homoclinic point of the orbit  $u_0'''$ , and the gray region indicates escaping orbits, while the red region gives the initial conditions (for  $z = 0$ ) of orbits that escape directly.

formed out of nothing. One orbit ( $u_0''$ ) is stable, and the other ( $u_0'''$ ) unstable (Fig. 18). This is called a "tangent bifurcation" (Contopoulos 2002).

From the unstable point  $u_0'''$  start two stable and two unstable asymptotic manifolds (Fig. 19a). The inner stable and unstable asymptotic manifolds surround the orbit  $u_0''$  and intersect at an infinite number of homoclinic points. The first homoclinic point is on the axis  $\dot{\rho} = 0$ , on the left of the orbit  $u_0''$ . The other couple of stable and unstable asymptotic curves approach the boundary and surround the orbit  $u_0'$  on the left of the figure.

Near the unstable orbit  $u_0'''$  and its homoclinic points there is some chaos (Figs. 18 and 19a). As  $E$  decreases several periodic orbits bifurcate from  $u_0''$  and near all the unstable orbits there are chaotic regions. These chaotic regions increase as  $E$  decreases. Two examples of bifurcating families, namely  $2/3$  and  $1/3$  are shown in Fig. 18. The orbit  $u_0''$  remains stable from its generation at  $E = 0.19236$  down to  $E = 0.1912$ . At  $E = 0.1912$  the orbit  $u_0''$  becomes unstable and a double period  $1/2$  stable orbit bifurcates there towards smaller values of  $E$ . In Fig. 19b this orbit has receded from  $u_0''$  and two islands of stability are formed, one around each point. The orbits of the islands go alternatively from one island to the other.

The orbit  $u_0''$  remains unstable for a small interval  $\Delta E$  and then it becomes again stable, generating an unstable periodic orbit  $1/2$ .

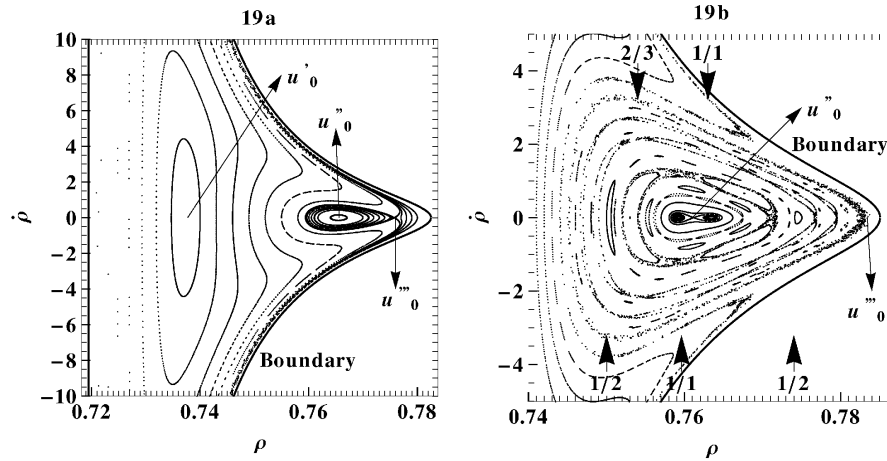


**Fig. 19** (19a) A surface of section  $(\rho, \dot{\rho})$  for  $E = 0.192$  (just below the value of  $E = 0.19236$  when the orbits  $u_0''$ ,  $u_0'''$  are formed at a tangent bifurcation). Invariant curves surround the orbits  $u_0''$ ,  $u_0'''$  and are also near the boundary. A little chaos appear near the unstable orbit  $u_0''$  and its asymptotic curves. (19b) A surface of section for  $E = 0.19045$ . It contains several islands around periodic orbits that have bifurcated from  $u_0''$ , like  $1/2$ ,  $2/3$  and  $1/1$ . Several chaotic regions appear between the islands, but they are separated from each other by invariant curves around  $u_0''$ . For this value of  $E$  the orbit  $u_0''$  is unstable, while the boundary (representing the orbit  $z = 0$ ) is stable.

As  $E$  comes close to  $E = 0.194045$  the family  $u_0''$  becomes again unstable for a small interval  $\Delta E$ . At the transition to instability it generates two different stable periodic orbits of equal period  $1/1$ . In Fig. 19b the orbit  $u_0''$  is unstable and the two islands around it refer to different orbits. For a little smaller  $E$  the orbit  $u_0''$  becomes again stable and generates two unstable periodic orbits  $1/1$ .

As  $E$  decreases further there is an infinity of transitions to instability and stability of orbits of double period  $1/2$  and of equal period  $1/1$ . At the limit of this infinite sequence of transitions the orbit  $u_0''$  reaches the escape region (Fig. 18) and does not exist for smaller values of  $E$ .

This phenomenon of infinite transitions to instability and stability along the same family was found also in other dynamical systems, e.g. the system given by Eq. (1) of the present paper (Contopoulos and Zikides 1980).

The chaotic regions of Fig. 19b are separated from each other by invariant curves closing around  $u_0''$ . For a little smaller  $E$  most of these invariant curves are destroyed, as  $E$  decreases, and a large chaotic region is formed (Figs. 18 and 20a) for  $E = 0.19015$ . This large chaotic region contains several islands of stability, like  $1/1$ ,  $1/2$ ,  $2/3$  etc (Fig. 20a), that recede from  $u_0''$  as  $E$  decreases (see the characteristics of the corresponding periodic orbits in Fig. 18).

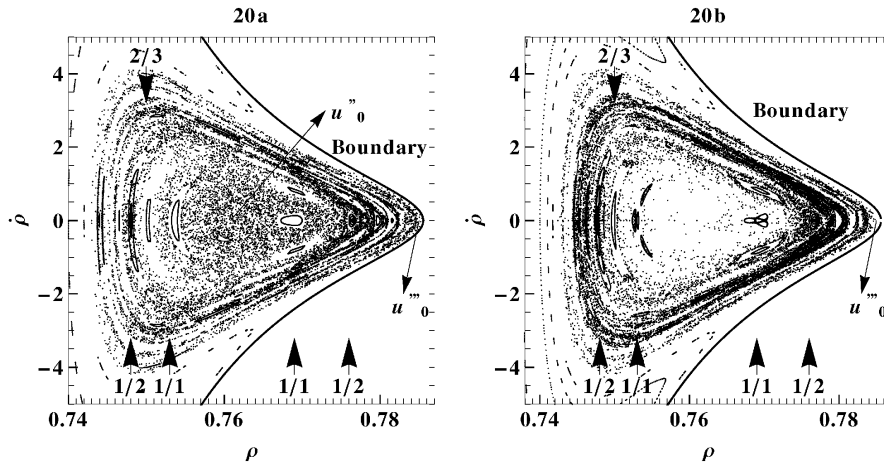


**Fig. 20** (20a) A surface of section  $(\rho, \dot{\rho})$  for  $E = 0.19015$ . In this case most of the chaotic regions have joined. However, there are also islands, like  $1/2$ ,  $2/3$ ,  $1/1$ . (20b) A surface of section for  $E = 0.1901$  below the escape value of  $E = E_{esc}$  where escapes start to appear. The chaotic region of Fig. 20a is now a region of escapes, but we see also the same islands.

## 5 Escapes from the Manko-Novikov system (2)

In the MN system (including the Kerr system) there are two types of escapes of orbits: (a) Escapes to infinity when  $E \gtrsim 1$ , and (b) escapes to the central bumpy black hole for small values of  $E$ .

The first type of escapes (escapes to infinity) is similar to the escapes in the Keplerian two-body problem (escapes along hyperbolic orbits). The permissible region increases in size as the energy increases. This size tends to infinity as the energy approaches the energy of the parabolic motions.

On the other hand, the escapes to the bumpy black hole occur when the CZVs open inwards as the energy decreases and allow motions towards the bumpy black hole.

In the MN case, that we study here, when  $E = 0.1901$  the CZV of the inner region (the outer region does not exist) joins two CZVs, above and below it and orbits from the inner region are allowed to escape to the bumpy black hole ( $\rho = 0$ ). The aforementioned CZVs above and below the central region are the second and fourth leaf-like CZVs respectively (counting clockwise) in Fig. 12 from the set of five CZVs touching the broken horizon of the bumpy black hole ( $\rho = 0$ ). These two CZVs expand outwards on both sides of the axis  $\dot{\rho} = 0$ , while  $E$  decreases, until (for  $E \approx 0.1901$ ) they reach the expanding central inner region (Fig. 18), which till then contains only bounded orbits. After the connection, orbits of the inner region may escape downwards (Fig. 21a) or upwards (Fig. 21b) to the central bumpy black hole.

In the MN case the escaping orbits are chaotic orbits that undergo chaotic scattering. In fact, if we compare Fig. 20a ( $E = 0.19015$ ) where no escapes are permitted, and Fig. 20b where we have many escapes we see a great similarity. That is the large chaotic domain around  $u_0$  of Fig. 20a is transformed into an escape domain in Fig. 20b. We see several islands in Fig. 20b that are slightly

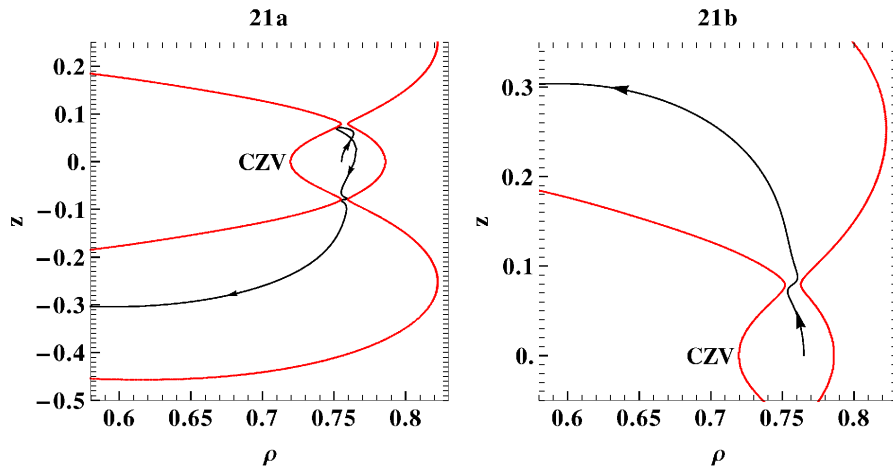


**Fig. 21** Escapes in the MN metric Fig. (21a) downwards ( $E = 0.1901$ ) and Fig. (21b) upwards ( $E = 0.1899$ ).

changed from the islands of Fig. 20a (the main change is that the islands 1/1 in Fig. 20a are surrounded by 3 secondary islands in Fig. 20b).

This similarity explains why the chaotic domain of Fig. 18 (around  $u_0''$ ) is transformed into an escape domain for  $E \leq 0.1901$ . In particular the periodic orbit  $u_0''$  of Fig. 20a reaches the point where the main CZV of the inner region joins the upper and lower CZVs and for smaller  $E$  this orbit escapes to the bumpy black hole, i.e. the periodic orbit does not exist any more.

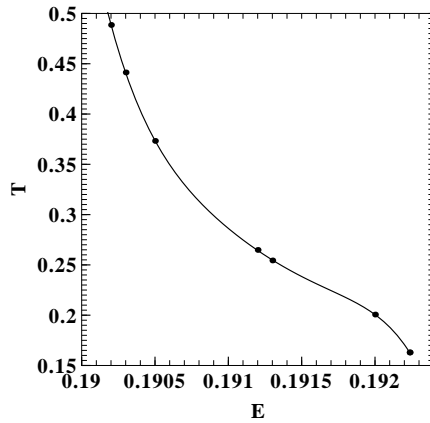


**Fig. 22** The period of the orbit  $u'_0$  as a function of the energy  $E$ .

This case is very similar to the cases  $y = \pm\sqrt{2x}$  (orbits (a) and (a')) of the system (1). There are two more similarities between the two cases. First is the sequence of infinite transitions to instability and stability of the orbits  $u'_0$  and the

orbits ( $a$ ) and ( $a'$ ). The second similarity is in the periods of the orbit  $u_0''$  and of the orbits ( $a$ ) and ( $a'$ ), which both tend to infinity as the orbits approach the termination point. The period of the orbits  $u_0''$  is given in Fig. 22, which increases considerably as  $E$  tends to  $E = 0.1901$  and presumably it tends to infinity. The period of the orbits  $y = \pm\sqrt{2x}$  was also found to tend to infinity (Contopoulos and Zikides 1980).

This behavior is consistent with the Strömberg termination principle of the families of periodic orbits (Szebehely 1967). According to this principle the families either join other families, or terminate when their size, or their energy, or their period becomes infinite.

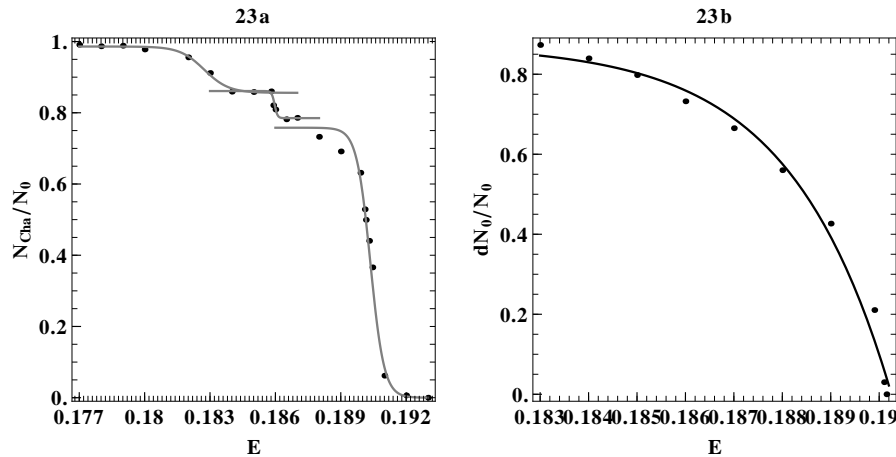


**Fig. 23** (23a) The proportion of the chaotic orbits (including the escape orbits), with initial conditions along the axis  $x$ , as a function of the energy  $E$ . (23b) The proportion  $dN_0/N_0$  of direct escapes as a function of  $E$ .

The proportion of chaotic + escaping orbits  $N_{cha}/N_0$  increases as the energy decreases (Fig. 23a). We calculate the proportion  $N_{cha}/N_0$  by taking initial conditions of orbits along the  $x$ -axis. This proportion tends to zero for relatively large  $E$  but it increases abruptly as  $E$  goes beyond  $E_{esc}$  (to smaller  $E$ ). An approximate formula for this proportion is

$$N_{cha}/N_o = 0.379[1 + \tanh(304 - 1597E)] \quad (17)$$

and can be applied in the interval  $0.188 < E < 0.192$  (Fig. 25). The curve (17) is very similar to the corresponding curve of the Hamiltonian (1) (Fig. 10a). However, for  $E \leq 0.186$  the proportion of escaping orbits increases further and tends to 100%. In Fig. 23a two more abrupt increases can be seen. The first of these two increases takes place near  $E \approx 0.186$ , and around it one can use an approximate formula  $N_{cha}/N_o = 0.823 + 0.038 \tanh(1399 - 7253E)$ . The second increase takes place near  $E \approx 0.183$  and the corresponding approximate formula is  $N_{cha}/N_o = 0.921 + 0.065 \tanh(163 - 892E)$ . This formula gives values near  $N_{cha}/N_o = 0.99$  for  $E < 0.180$ .

When  $E < E_{esc}$  most chaotic orbits escape to the bumpy black hole. However, only a proportion  $dN_0/N_0$  escape directly from the system without any further intersection with the axis  $z = 0$ . This proportion increases as the energy  $E$  decreases (Fig. 23b). The curve  $dN_0/N_0$  of Fig. 23b is very similar to the corresponding curve of Fig. 10b. In Fig. 18 we mark in red the initial conditions of the directly escaping orbits. Most of the other chaotic orbits escape after one or more intersections beyond the original point, with the  $z = 0$  axis. But, as we see in Fig. 18, for  $E < E_{esc}$  there are also orbits that do not escape. In particular the periodic orbit  $u'_0$  and orbits close to it do not escape for much smaller values of  $E$ . Similarly the orbits that bifurcated from  $u''_0$ , like the orbits  $1/3$ ,  $1/2$ ,  $2/3$ ,  $1/1$  (Fig. 18) exist also for  $E < E_{esc}$ . However, all these families become unstable for small  $E$ . In any case the existence of an infinity of families of unstable periodic orbits is a similar phenomenon as the one observed in the system (1).

## 6 Conclusions

We considered the periodic orbits and escapes in two quite different dynamical systems in order to find their common features. The first system is a system of two coupled oscillators, while the second system is a perturbation of the Kerr metric in General Relativity.

In the system (1) escapes occur when the Curves of Zero Velocity open and many orbits escape to infinity. In the second case we have escapes to infinity, but we emphasized the escapes to the central bumpy black hole. In both cases when the energy changes and reaches the escape value, there is a periodic orbit that approaches the point where the CZV opens and its period tends to infinity. Thus, the family of periodic orbits terminates at the escape energy. Before the escape energy this family undergoes an infinity of transitions from stability to instability and vice-versa, and at every transition there is a bifurcation of an equal or double period family of periodic orbits, that does not escape as the energy varies.

It seems that, in general, in systems with escapes there is a family of periodic orbits that terminates at infinite period when the CZVs open.

Another common feature is that most chaotic orbits become escape orbits beyond the escape energy (beyond means larger energy in the first system, but smaller energy in the second system). However, for energies slightly beyond the escape energy most orbits take a rather long time to escape. As the energy increases (decreases) the proportion of fast escapes increases considerably. The proportion of chaotic (+ escaping) orbits increases abruptly as the energy goes beyond the escape energy.

We studied the structure of the phase space and we distinguished the ordered and chaotic domains. The ordered domains surround the positions of the stable periodic orbits. Thus we found these periodic orbits and their bifurcations as the energy varies. On the other hand, the chaotic domains surround the asymptotic curves from the unstable periodic orbits.

As the two systems under study are quite different we studied them in detail separately.

In the first case (of two coupled oscillations) we found the characteristics of the periodic orbits and their stability. Then we found the structure of the phase space on a surface of section for various values of the energy. As the energy increases the

chaotic domains increase, while all stable periodic orbits become unstable. (However, new stable periodic orbits appear for larger energies at tangent bifurcations.)

The chaotic domains are covered by the asymptotic curves of a main unstable periodic orbit. As the energy goes beyond the escape energy most chaotic orbits escape, either directly, or after a small or a large number of intersections with the  $y=0$  axis. Some asymptotic curves are split into successive pieces, each piece making infinite rotations around an escape domain.

The statistics of chaos and escape are given by different graphs: (a) (b) the proportion of chaotic and escaping orbits and the proportion of the directly escaping orbits as functions of the energy, (c) (d) the proportion of the escaping orbits at the  $n$ th intersection with respect to the initial total number of orbits and with respect to the remaining orbits, as functions of the number of iterations (which represents time).

In the system (2) (Manko-Novikov metric) we found various forms of the CZVs for various values of the energy, and the corresponding simple periodic orbits. We found also surfaces of section with mostly ordered orbits, for relatively large energies  $E$  (but  $E < 1$ ), or a mixture of ordered and chaotic orbits for smaller energies. We found the characteristics of the main families of periodic orbits and their bifurcations.

We emphasized the appearance of a couple of periodic orbits (one stable, and one unstable) at a tangent bifurcation, and their evolution. As the energy decreases the stable family undergoes an infinity of bifurcations (at transitions from stability to instability and vice versa). As the energy goes below a critical value the period of this orbit goes to infinity and then this orbit escapes to the bumpy black hole and this family of periodic orbits terminates.

On the other hand, the bifurcating families exist and do not escape, but become unstable. We found the proportion of the chaotic regions as the energy decreases. Beyond the critical energy most of the chaotic region contains escape orbits. The proportion of the chaotic+escaping orbits increases abruptly below the escape energy and tends to 100% for smaller energies.

It is remarkable that these quite different systems have very similar forms of the proportion of chaotic orbits (Figs. 10a and 23a) and of the proportion of directly escaping orbits (Figs. 10b and 23b). The relations of the periodic orbits with the chaotic and escaping orbits are also quite similar. These similarities indicate that the properties of periodic, ordered, chaotic and escaping orbits that we studied in the present paper are very similar in generic dynamical systems.

**Acknowledgements** G. Lukes-Gerakopoulos was supported in part by the Research Committee of the Academy of Athens and by the DFG grant SFB/Transregio 7.

## References

- Apostolatos, T. A., Lukes-Gerakopoulos, G., Contopoulos G.: How to Observe a Non-Kerr Spacetime Using Gravitational Waves. *Phys. Rev. Lett.* 103, 111101 (2009). doi:10.1103/PhysRevLett.103.111101
- Bambi, C.: Constraint on the quadrupole moment of super-massive black hole candidates from the estimate of the mean radiative efficiency of AGN. *Phys. Rev. D* 83, 103003 (2011). doi:10.1103/PhysRevD.83.103003

- Bambi, C., Barausse, E.: Constraining the Quadrupole Moment of Stellar-mass Black Hole Candidates with the Continuum Fitting Method. *Astrophys. J.* 731, 121 (2011a). doi:10.1088/0004-637X/731/2/121
- Bambi, C., Barausse, E.: Final stages of accretion onto non-Kerr compact objects. *Phys. Rev. D* 84, 084034 (2011b). doi:10.1103/PhysRevD.84.084034
- Benet, L., Trautman, D., Seligman, T.: Chaotic Scattering in the Restricted Three-Body Problem. I. The Copenhagen Problem. *Celest. Mech. Dyn. Astron.* 66, 203-228 (1996). doi:10.1007/BF00054965
- Benet, L., Seligman, T., Trautman, D.: Chaotic Scattering in the Restricted Three-Body Problem II. Small mass parameters. *Celest. Mech. Dyn. Astron.* 71, 167 (1998). doi:10.1023/A:1008335232601
- Bleher, S., Grebogi, C., Ott, E., Brown, R.: Fractal boundaries for exit in Hamiltonian dynamics. *Phys. Rev. A* 38, 930-938 (1988). doi:10.1103/PhysRevA.38.930
- Churchill, R., Pecelli, G., Rod, D.: Isolated unstable periodic orbits. *J. Differ. Equ.* 17, 329-348 (1975). doi:10.1016/0022-0396(75)90047-9
- Carter, B.: Global Structure of the Kerr Family of Gravitational Fields. *Phys. Rev.* 174, 1559-1571 (1968). doi:10.1103/PhysRev.174.1559
- Contopoulos, G.: Asymptotic curves and escapes in Hamiltonian systems. *Astron. Astrophys.* 231, 41-55 (1990)
- Contopoulos, G.: Order and chaos in dynamical astronomy. Springer, Berlin (2002)
- Contopoulos, G., Efsthathiou, K.: Escapes and Recurrence in a Simple Hamiltonian System. *Celest. Mech. Dyn. Astron.* 88, 163-183 (2004). doi:10.1023/B:CELE.0000016816.87061.11
- Contopoulos, G., Harsoula, M.: Stickiness in Chaos. *Int. J. Bifurc. Chaos* 18, 2929 (2008). doi:10.1142/S0218127408022172
- Contopoulos, G., Harsoula, M.: Stickiness effects in chaos. *Cel. Mech. Dyn.* 107, 77 (2010). doi:10.1007/s10569-010-9282-6
- Contopoulos, G., Kaufmann, D.: Types of escapes in a simple Hamiltonian system. *Astron. Astrophys.* 253, 379-388 (1992)
- Contopoulos, G., Zikides, M.: Periodic orbits and ergodic components of a resonant dynamical system. *Astron. Astrophys.* 90, 198-203 (1980)
- Contopoulos, G., Kandrup, H. E., Kaufmann D.: Fractal properties of escape from a two-dimensional potential. *Phys. D* 64, 310 (1993). doi:10.1016/0167-2789(93)90262-Y
- Contopoulos, G., Papadaki, H., Polymilis, C.: The structure of chaos in a potential without escapes. *Celest. Mech. Dyn. Astron.* 60, 249 (1994). doi:10.1007/BF0069332
- Contopoulos, G., Lukes-Gerakopoulos, G., Apostolatos, T. A.: Orbits in a Non-Kerr Dynamical System. *Int. J. Bifurc. Chaos* 21, 2261 (2011). doi:10.1142/S0218127411029768
- Cristadoro, G., Ketzmerick R.: Universality of Algebraic Decays in Hamiltonian Systems. *Phys. Rev. Lett.* 100, 184101 (2008). doi:10.1103/PhysRevLett.100.184101
- Eckhardt, B.: Irregular scattering. *Phys. D* 33, 89-98 (1988). doi:10.1016/S0167-2789(98)90012-4
- Eckmann, J.-P.: Roads to turbulence in dissipative dynamical systems. *Rev. Mod. Phys.* 53, 643-654 (1981). doi:10.1103/RevModPhys.53.643
- Gair, J. R., Li, C., Mandel, I.: Observable properties of orbits in exact bumpy spacetimes. *Phys. Rev. D* 77, 024035 (2008). doi:10.1103/PhysRevD.77.024035

- Heggie, D. C.: On the bifurcations of a certain family of periodic orbits. *Celest. Mech. Dyn. Astron.* 29, 207-214 (1983). doi:10.1007/BF01229135
- Hénon, M.: La diffusion chaotique. *Rech.* 209, 490-498 (1989).
- Jung, C., Scholz, H.: Cantor set structures in the singularities of classical potential scattering. *J. Phys. A* 21, 3607-3617 (1988). doi:10.1088/0305-4470/20/12/015
- Kerr, R. P.: Gravitational Field of a Spinning Mass as an Example of Algebraically Special Metrics. *Phys. Rev. Lett.* 11, 237-238 (1963). doi:10.1103/PhysRevLett.11.237
- Lukes-Gerakopoulos, G., Apostolatos, T. A., Contopoulos, G.: Observable signature of a background deviating from the Kerr metric. *Phys. Rev. D* 81, 124005 (2010). doi:10.1103/PhysRevD.81.124005
- Manko, V. S., Novikov, I. D.: Generalizations of the Kerr and Kerr-Newman metrics possessing an arbitrary set of mass-multipole moments. *Class. Quantum Gravity* 9, 2477-2487 (1992). doi:10.1088/0264-9381/9/11/013
- Newhouse, S.E.: Quasi-elliptic periodic points in conservative dynamical systems. *Am. J. Math.* 99, 1061-1087 (1977)
- Newhouse, S. E.: The creation of non-trivial recurrence in the dynamics of diffeomorphisms. In: Iooss, G., Helleman, R. H. G., Stora, R. (eds.) *Chaotic Behaviour of Deterministic Systems*, pp. 381-442. North-Holland, Amsterdam (1983)
- Ott, E., Tél, T.: Chaotic scattering: An introduction. *Chaos* 3, 417-426 (1993). doi:10.1063/1.165949
- Petit, J.-M., Hénon, M.: Satellite encounters. *Icarus* 66, 536-555 (1986). doi:10.1016/0019-1035(86)90089-8
- Psaltis, D., Johannsen, T.: A Ray-Tracing Algorithm for Spinning Compact Object Spacetimes with Arbitrary Quadrupole Moments. I. Quasi-Kerr Black Holes. <http://arxiv.org/abs/1011.4078> (2010)
- Siopis, C. V., Contopoulos, G., Kandrup, H. E.: Escape Probabilities in a Hamiltonian with Two Channels of Escape. *New York Acad. Sci. Ann.* 751, 205 (1995). doi:10.1111/j.1749-6632.1995.tb27523.x
- Siopis, C. V., Kandrup, H. E., Contopoulos, G., Dvorak, R.: Universal Properties of Escape. *New York Acad. Sci. Ann.* 773, 221 (1995). doi:10.1111/j.1749-6632.1995.tb12171.x
- Siopis, C. V., Kandrup, H. E., Contopoulos, G., Dvorak, R.: Universal properties of escape in dynamical systems. *Celest. Mech. Dyn. Astron.* 65, 57-681 (1996). doi:10.1007/BF00048438
- Szebehely, V.: *Theory of Orbits*. Academic Press, New York (1967)
- Veneroles, R.: Universality of Algebraic laws in Hamiltonian Systems. *Phys. Rev. Lett.*, 102, 64101 (2009). doi:10.1103/PhysRevLett.102.064101